

Qubits with electrons on liquid helium

M.I. Dykman^{1,*}, P.M. Platzman², and P. Seddighrad¹

¹*Department of Physics and Astronomy, Michigan State University, East Lansing, MI 48824*

²*Bell Laboratories, Lucent Technologies, Murray Hill, New Jersey 07974*

(Dated: February 1, 2008)

We study dissipation effects for electrons on the surface of liquid helium, which may serve as qubits of a quantum computer. Each electron is localized in a 3D potential well formed by the image potential in helium and the potential from a submicron electrode submerged into helium. We estimate parameters of the confining potential and characterize the electron energy spectrum. Decay of the excited electron state is due to two-ripplon scattering and to scattering by phonons in helium. We identify mechanisms of coupling to phonons and estimate contributions from different scattering mechanisms. Even in the absence of a magnetic field we expect the decay rate to be $\lesssim 10^4 \text{ s}^{-1}$. We also calculate the dephasing rate, which is due primarily to ripplon scattering off an electron. This rate is $\lesssim 10^2 \text{ s}^{-1}$ for typical operation temperatures.

PACS numbers: 03.67.Lx, 73.21.-b, 76.60.Es, 73.63.-b

I. INTRODUCTION

Much interest has attracted recently the idea of creating a condensed-matter based quantum computer (QC). A major challenge is to have a system that would have a sufficiently long relaxation time and nevertheless could be controlled with high precision and allow its quantum state to be measured. The proposed systems include localized electron spins in semiconductor heterostructures [1, 2, 3], nuclear spins of ^{31}P donors [4] or ^{29}Si nuclei [5] in a zero nuclear spin ^{28}Si matrix, electron states in a quantum dot excited by terahertz radiation [6], excitons in quantum dots [7, 8], Josephson-junction based systems [9, 10, 11, 12, 13, 14], electrons on helium surface [15, 16], quantum dots coupled via a linear support [17], and trapped polar molecules [18].

The system of electrons on the surface of superfluid ^4He is attractive, from the point of view of making a scalable quantum computer, because (i) it has already been extensively studied theoretically and experimentally [19], (ii) the electrons have extremely long relaxation time: they display the highest mobility known in a condensed-matter system [20], and (iii) the inter-electron distance is comparatively large, $\sim 1 \mu\text{m}$. To make a QC we suggested [15, 16] to fabricate a system of micro-electrodes, which would be submerged beneath the helium surface. Each electrode is supposed to localize one electron above it, as seen in Fig. 1, and to control this electron.

The two states of an electron qubit are the two lowest states of quantized motion transverse to the surface. To further slow down the already slow relaxation, we initially proposed to apply a magnetic field B_\perp normal to the surface. Then the estimated relaxation time T_2 becomes as small as 10^{-4} s , for typical $B_\perp \sim 1.5 \text{ T}$ and

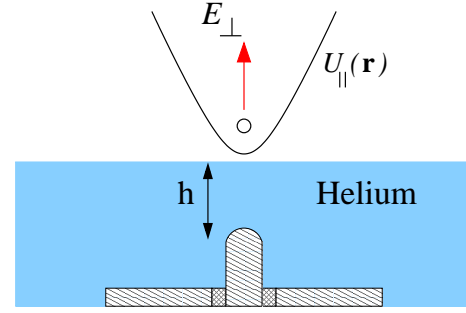


FIG. 1: A sketch of a micro-electrode submerged by the depth $h \sim 0.5 \mu\text{m}$ beneath the helium surface, with an electron localized above it. The electron is driven by a field E_\perp normal to the surface. This field comes from the electrode and the parallel-plate capacitor (only the lower plate of the capacitor is shown). The in-plane electron potential $U_\parallel(\mathbf{r})$ is parabolic near the minimum, with curvature determined by the electrode potential ($\mathbf{r} = (x, y)$ is the in-plane position vector).

temperatures $T \approx 10 \text{ mK}$, whereas the clock frequency of the computer Ω can be in the GHz range. This attracted attention of experimentalists to the project [21, 22, 23].

In this paper we show that, even without a magnetic field, the relaxation rate of a confined electron can be much less than that of a free electrons. The dephasing rate can be even smaller than the previous estimate for a strong magnetic field. This is due to large level spacing in a 3D confining potential formed by a localizing micro-electrode provided the electrode is sufficiently thin. Electrodes of an appropriate shape have already been fabricated [22].

For low temperatures, the major known dissipation mechanism is scattering by surface capillary waves, ripples. These waves are very slow. Therefore a large distance between electron energy levels makes it impossible to conserve energy and momentum in a one-ripplon

*Electronic address: dykman@pa.msu.edu

decay process. Decay of the excited electron state, i.e. electron energy relaxation may occur via scattering into two short-wavelength ripples. We show that a very important role is played also by decay processes, where the electron energy goes to phonons in helium. Such phonons propagate nearly normal to the surface. We identify the major mechanisms of electron-phonon coupling and analyze their contribution to the decay rate. Dephasing is due primarily to scattering of thermally excited ripples off an electron. We find its temperature dependence for different coupling mechanisms. We also investigate the spectrum of sideband absorption in which a microwave-induced electron transition is accompanied by creation or annihilation of a ripplon, and analyze the related decrease of the intensity of the zero-ripplon absorption line.

In Sec. II below we analyze the energy spectrum of a confined electron and discuss many-electron effects. In Sec. III we discuss energy relaxation rate for different mechanisms of electron-ripplon and electron-phonon coupling. In Sec. IV we consider dephasing rate. Sec. V deals with one-ripplon sidebands and the Debye-Waller type factor in the zero-ripplon absorption line. In Sec. VI we discuss electron relaxation and dephasing from fluctuations in the underlying electrodes. Sec. VII contains concluding remarks.

II. ELECTRON STATES IN ONE- AND MANY-ELECTRON SYSTEMS

A. Single-electron energy spectrum

The quantum computer considered in this paper is based on a set of electrons which reside in potential wells in free space above helium, cf. Fig. 1. The electrons are prevented from penetrating into helium by a high potential barrier ~ 1 eV at the helium surface. For one electron, the potential well is formed by the electrostatic image in helium, the potential from the electrode, and also the potential created by the grounded plate and a parallel plate above the electron layer (the latter is not shown in Fig. 1).

We assume that the helium occupies the halfspace $z \leq 0$. The image potential for an electron is $-\Lambda/z$, where $\Lambda = (\epsilon - 1)e^2/4(\epsilon + 1)$, with $\epsilon \approx 1.057$ being the dielectric constant of helium. The energy spectrum for 1D motion in such a potential is hydrogenic,

$$E_n = -R/n^2 \quad (n = 1, 2, \dots), \quad R = \Lambda^2 m/2\hbar^2. \quad (1)$$

The effective Rydberg energy R is ≈ 8 K, and the effective Bohr radius is $r_B = \hbar^2/\Lambda m \approx 76$ Å (m is the electron mass).

The electrode potential leads to Stark shift of the energy levels (1) [24] and to quantization of motion parallel to the surface. A realistic estimate of this potential and of the electron energy spectrum can be made by modelling the electrode as a conducting sphere with a diameter $2r_{\text{el}}$ equal to the electrode diameter. The center of

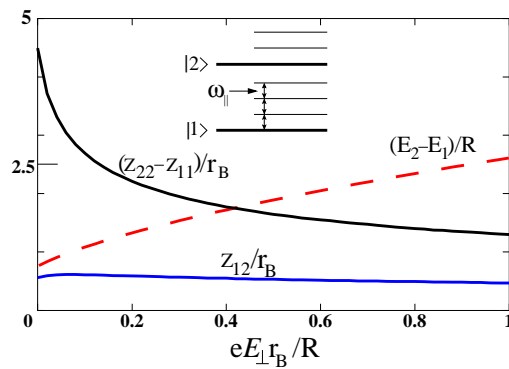


FIG. 2: Energy difference $E_2 - E_1$ and matrix elements $z_{nm} = \langle n|z|m \rangle$ of the electron coordinate normal to helium surface on the wave functions of the ground and first excited states of motion in the z -direction, $|1\rangle$ and $|2\rangle$, vs. the overall pressing field E_\perp . The scaled field $eE_\perp r_B/R = 1$ for $E_\perp \approx 0.91$ kV/cm. The inset shows the full energy level diagram. Each level E_n of z -motion gives rise to a set of energy levels of vibrations parallel to helium surface, with typical spacing $\hbar\omega_\parallel$.

the sphere is located at depth h beneath the helium surface. Typically we expect h to be ~ 0.5 μm , so that it largely exceeds the distance from the electron to the surface $\sim r_B$. For $z \ll h$ and for the in-plane distance from the electrode $r \equiv (x^2 + y^2)^{1/2} \ll h, (h^2 - r_{\text{el}}^2)^{1/2}$, the electron potential energy is

$$U(\mathbf{r}, z) \approx -\frac{\Lambda}{z} + e\mathcal{E}_\perp z + \frac{1}{2}m\omega_\parallel^2 r_\parallel^2, \quad (2)$$

with

$$\begin{aligned} \mathcal{E}_\perp &= V_{\text{el}} r_{\text{el}} h^{-2} + e r_{\text{el}} h (h^2 - r_{\text{el}}^2)^{-2}, \\ \omega_\parallel &= (e\mathcal{E}_\perp / m\hbar)^{1/2}. \end{aligned} \quad (3)$$

Here, $\mathbf{r} = (x, y)$ is the electron in-plane position vector, and V_{el} is the electrode potential. The second term in \mathcal{E}_\perp comes from the image of the electron in the spherical electrode.

In the approximation (2), the electron out-of-plane and in-plane motions separate, with in-plane motion being just harmonic oscillations. Variational calculations of the energy spectrum of the out-of-plane motion were done earlier [24]. The simple model (2) with an infinite wall at $z = 0$ describes the observed transition frequencies with an error of only a few percent, which is sufficient for the present purposes (more realistic models have been discussed in literature, see Refs. 26, 27 and papers cited therein). The full electron energy spectrum in the potential (2) is sketched in the inset in Fig. 2. The two states of a qubit are the ground and first excited states of motion transverse to the surface, $|1\rangle$ and $|2\rangle$, both corresponding to the ground state of in-plane vibrations.

In what follows, we characterize the electron state $|i, \nu, m_\nu\rangle$ with the following 3 quantum numbers: $i =$

1, 2 enumerates the state of out-of-plane motion, $\nu = 0, 1, \dots$ gives the energy level of in-plane vibrations, and $m_\nu = 0, 1, \dots, \nu$ enumerates degenerate vibrational states within this level.

B. Choosing parameters of the many-electron system

1. Working frequency considerations

For a multi-qubit multi-electrode QC, the depth h by which the controlling electrodes are submerged into helium, the inter-electrode distances d_{ij} , and the electrode potentials should be chosen in a way that would optimize performance of the QC. This includes, in the first place, having a high working frequency Ω_{QC} and low relaxation rate Γ . The frequency Ω_{QC} is limited by the rate of single-qubit operations and by the rate of excitation transfer between neighboring qubits, which is determined by the qubit-qubit interaction.

Single-qubit operations will be performed [15] by applying pulses of resonant microwave radiation, which cause transitions between the states $|1\rangle$ and $|2\rangle$. The corresponding Rabi frequency is $\Omega_R = e\mathcal{E}_m|z_{12}|/\hbar$, where \mathcal{E}_m is the field amplitude. As seen from Fig. 2, $|z_{12}|/r_B \gtrsim 0.5$, and therefore even a comparatively weak field $\mathcal{E}_m = 1 \text{ V/cm}$ gives $\Omega_R \gtrsim 6 \times 10^8 \text{ s}^{-1}$. This shows that single-qubit operations should not limit Ω_{QC} at least at the level of $10^7 - 10^8 \text{ Hz}$.

Because the wave functions of different electrons do not overlap, the interaction between the qubits that we consider is dipolar, as in liquid-state NMR quantum computers [28]. An important feature of electrons on helium is that their localization length normal to the surface r_B greatly exceeds the atomic radius, which makes the dipole-dipole interaction orders of magnitude stronger than the dipolar interaction in atomic systems.

Of interest to us is the part of the qubit-qubit interaction that depends on the states of the qubits. Two types of dipole moments have to be distinguished. One is determined by the difference $z_{11} - z_{22}$ of average distances of the electron from helium surface in the states $|1\rangle$ and $|2\rangle$. The dipole moment $e(z_{11} - z_{22})$ does not depend on time, if we take into account time dependence of the wave functions, it can be called “static”. The interaction energy between the static dipoles of the i th and j th qubits can be written as $(1/4)U_{ij}^{(\text{st})}\sigma_z^i\sigma_z^j$, where $\sigma_z^i = |2\rangle_i\langle 2|_i - |1\rangle_i\langle 1|_i$ is the operator of the difference of the state occupations for the i th qubit, and

$$U_{ij}^{(\text{st})} = e^2|z_{22} - z_{11}|^2/d_{ij}^3. \quad (4)$$

The other dipole moment is associated with the $1 \rightarrow 2$ transition. If we use time-dependent wave functions, it oscillates in time at high frequency $\Omega_{12} = (E_2 - E_1)/\hbar$. Resonant interaction between such oscillating dipoles has energy $(1/4)U_{ij}^{(\text{osc})}[\sigma_+^i\sigma_-^j + H.c.]$, where $\sigma_+^i = [\sigma_-^i]^\dagger =$

$2|2\rangle_i\langle 1|_i$ is the $1 \rightarrow 2$ transition operator for the i th qubit, and

$$U_{ij}^{(\text{osc})} = e^2|z_{12}|^2/d_{ij}^3. \quad (5)$$

The interaction between static and oscillating dipoles is nonresonant and can be safely neglected.

The interactions (4) and (5) allow implementation of a CNOT two-qubit gate and of interqubit excitation transfer, respectively [15, 16]. For a typical dipole moment er_B , the interaction energy $e^2r_B^2/d_{ij}^3$ between the qubits separated by $d_{ij} = 1 \mu\text{m}$ is $2 \times 10^7 \text{ Hz}$, in frequency units. This energy is very sensitive to d_{ij} and can be increased by reducing the inter-electron distance. Eqs. (4), (5) apply for d_{ij} less than the distance from the electrons to the grounded plate in Fig. 1; for larger d_{ij} the interaction is screened and falls down as d_{ij}^{-5} . In practice it means that the interqubit coupling is likely to be limited to nearest and probably next nearest neighbors.

The matrix elements z_{nm} depend on the overall field E_\perp that presses electrons against the helium surface. They can be obtained by solving a one-dimensional Schrödinger equation for the potential $-\Lambda z^{-1} + eE_\perp z$ with a hard wall at $z = 0$ [cf. Eq. (2); we note that the total field E_\perp differs from the field \mathcal{E}_\perp produced by one electrode, see below]. The results are shown in Fig. 2.

The difference $z_{22} - z_{11}$ sharply decreases with increasing field for small E_\perp because of field-induced squeezing of the wave functions, which is particularly strong for the wave function of the excited state $|2\rangle$. The interplay between the squeezing and better overlapping of the wave functions $|1\rangle$ and $|2\rangle$ with increasing field leads to a weak field dependence of z_{12} for $eE_\perp r_B/R \lesssim 1$. It is seen from Fig. 2 and Eq. (4) that, for weak pressing field $E_\perp < 300 \text{ V/cm}$, the energy of the “static” interaction is higher than its estimate given above by a factor varying from 20 to 4 with increasing E_\perp , because of the large numerical value of $(z_{22} - z_{11})/r_B$. It is also significantly higher than the energy given by Eq. (5).

In a multi-qubit system, the fields \mathcal{E}_\perp on different electrodes are used to tune targeted qubits in resonance with microwave radiation and with each other. In the simple case of one microwave frequency, all these fields are nearly the same, they differ by $\sim 1 \text{ V/cm}$, or $\sim 1\%$. Therefore in Eqs. (4), (5) we assumed that the matrix elements z_{nm} are the same for different qubits. Overall, for inter-electron distances $d \lesssim 1 \mu\text{m}$, the qubit-qubit interaction limits the clock frequency of the quantum computer Ω_{QC} to $10^7 - 10^8 \text{ Hz}$.

2. Limitations from many-electron effects

The electron energy spectrum should be formed so as to minimize the electron relaxation rate. One of the most “dangerous” relaxation processes is quasi-elastic scattering by capillary waves on helium surface, ripplons, in which an electron makes a transition between its states

and a ripplon is emitted or absorbed. This scattering is responsible for finite electron lifetime T_1 . Typical energies of appropriate ripplons are extremely small, $\sim 10^{-3}$ K (see below). Therefore the scattering can be eliminated for a one-qubit system, if none of the excited vibrational levels of the state $|1\rangle$ is in resonance with the ground vibrational level of the state $|2\rangle$ shown with a bold line in Fig. 2.

From Eq. (3), for a field $\mathcal{E}_\perp = 500$ V/cm and $h = 0.5 \mu\text{m}$ we have $\omega_\parallel/2\pi \approx 2.1 \times 10^{10}$ Hz ≈ 1.0 K. Even though the spacing between vibrational levels is less than the energy gap $E_2 - E_1 \sim 6 - 10$ K, with so big ω_\parallel it is easy to avoid resonance between E_2 and an excited vibrational level of the state 1, i.e. between $E_2 - E_1$ and $n\hbar\omega_\parallel$.

The situation becomes more complicated for a system of interacting qubits. The interaction leads to coupling of in-plane vibrations of different electrons. In a many-electron system the vibrational energy spectrum becomes nearly continuous. One can think that each vibrational level in Fig. 2 becomes a bottom of a band of in-plane vibrational excitations. We will assume that the width of the lowest band Δ_\parallel is small compared to ω_\parallel . The width of the ν th band is then $\sim \nu\Delta_\parallel$ for not too large ν . To avoid quasi-elastic scattering by ripplons, the electron energy spectrum has to be discrete, i.e. vibrational bands should be well separated from each other up to energies $E_2 - E_1$, that is for $\nu \sim (E_2 - E_1)/\hbar\omega_\parallel$. This means that

$$\Delta_\parallel \ll \hbar\omega_\parallel^2/(E_2 - E_1). \quad (6)$$

The value of Δ_\parallel depends on the geometry of the many-electron system. It can be found if the electrodes and the electrons above them form a regular 2D array, or in other words, the electrons form a Wigner crystal with the same lattice constant as the electrodes. Then, if the phonon frequencies of the free-standing crystal in the absence of the electrode potential are $\omega_{\mathbf{k}j}$ (\mathbf{k} is the wave vector and $j = 1, 2$ is the branch number), then the vibrational frequencies of the pinned crystal are $(\omega_{\mathbf{k}j}^2 + \omega_\parallel^2)^{1/2}$. The phonon bandwidth is small compared to ω_\parallel provided $\omega_{\mathbf{k}j} \ll \omega_\parallel$, in which case $\Delta_\parallel = \max \omega_{\mathbf{k}j}^2/\omega_\parallel \sim \omega_p^2/\omega_\parallel$, where $\omega_p = (2\pi e^2 n_e^{3/2}/m)^{1/2}$ is the characteristic zone-boundary frequency of the free-standing Wigner crystal (n_e is the electron density).

It follows from the above arguments and the condition (6) that quasi-elastic scattering will be eliminated for a pinned Wigner crystal provided

$$\omega_p^2 \ll \hbar\omega_\parallel^3/(E_2 - E_1). \quad (7)$$

This imposes an upper limit on the nearest neighbor spacing $d = \min d_{ij}$, because $\omega_p \propto d^{-3/2}$. For a square lattice with $d = 1 \mu\text{m}$ we have $\omega_p/2\pi \approx 6.3$ GHz.

For the multi-electrode system, the frequency ω_\parallel itself depends on the inter-electrode distance d . If the electrode radius r_{el} is small compared to the depth h , the effect of the electrostatic image in the electrode [in particular,

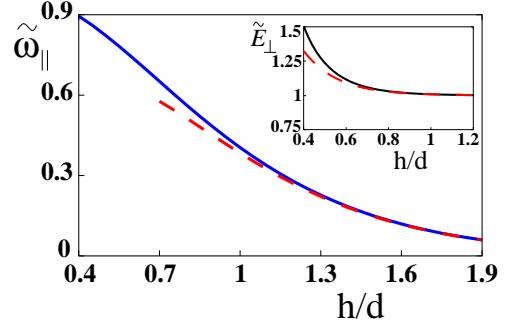


FIG. 3: In-plane frequency $\tilde{\omega}_\parallel = \omega_\parallel/\omega'_\parallel$ and normal to the surface field $\tilde{E}_\perp = E_\perp/E'_\perp$ for an electron above a square array of electrodes. The electron is localized at height h above one of the electrodes. The inter-electrode spacing is d . Electrodes are modelled by small spheres, $r_{\text{el}}/h \ll 1$, with same positive potential V_{el} . The scaling frequency $\omega'_\parallel = (eV_{\text{el}}r_{\text{el}}/mh^3)^{1/2}$ is given by Eq. (3) and corresponds to the limit $d \rightarrow \infty$. The scaling field is $\tilde{E}_\perp = 2\pi n_e V_{\text{el}} r_{\text{el}}$. Asymptotic behavior of $\tilde{\omega}_\parallel$ and \tilde{E}_\perp for large $2\pi h/d$ is shown with dashed lines.

the second term in Eq. (3) for \mathcal{E}_\perp] can be ignored. The overall potential of the electrode lattice at a distance z above helium surface ($z + h > 0$) is

$$V(\mathbf{r}, z) = 2\pi n_e V_{\text{el}} r_{\text{el}} \sum_{\mathbf{G}} G^{-1} \exp(i\mathbf{G}\mathbf{r}) e^{-G(z+h)} - 2\pi n_e V_{\text{el}} r_{\text{el}} (z + h) \quad (8)$$

where \mathbf{G} is the reciprocal lattice vector.

The dependence of ω_\parallel on h/d for a square electrode array is shown in Fig. 3 along with the z -dependence of the total normal field from the electrodes. The electrostatic in-plane confinement is due to the spatial nonuniformity of the electrode potential. Therefore ω_\parallel falls down as $2\pi(2eV_{\text{el}}r_{\text{el}}/md^3)^{1/2} \exp(-\pi h/d)$ for large $2\pi h/d$. However, as seen from Fig. 3, ω_\parallel remains close to the single-electrode value (3) for $h/d \lesssim 0.5$. This gives the desirable range of the aspect ratio h/d .

The total perpendicular field on a localized electron E_\perp comes from the electrodes and the capacitor that holds the system (its lower plate is shown in Fig. 1). As we will see, the field-induced squeezing of the electron wave functions (cf. Fig. 2) makes a significant effect on the electron relaxation rate. Therefore E_\perp should be minimized in order to reduce relaxation effects. At the same time, the electrostatic confinement (the frequency ω_\parallel) increases with the increasing field from the electrodes. It would be good to compensate the out-of-plane field E_\perp while keeping the in-plane potential as strongly confining as possible. This can be accomplished using the field from the capacitor, which is uniform in the plane and does not affect in-plane confinement.

The limitation on the compensating capacitor field comes from the condition that the overall field behind the

electron layer should attract electrons to helium, otherwise they will leave the surface. This field is formed not only by the externally applied potentials, but also by the electron layer itself. The total averaged over \mathbf{r} applied field in the electron plane should therefore exceed $4\pi en_e$. In other words, the uniform component $2\pi n_e V_{el} r_{el}$ of the electrode field $-\partial_z V|_{z=0}$ (8) can be compensated down to $4\pi en_e$. The remaining pressing field on the electron E_\perp becomes then $C \times 2\pi n_e V_{el} r_{el} + 4\pi en_e$ with small C ($C \approx 0.24$ for $h/d = 0.5$, as seen from Fig. 3).

We note that the frequency ω_\parallel can be further increased electrostatically without increasing E_\perp by using a more sophisticated configuration of electrodes. Analysis of such configurations is outside the scope of this paper. We note also that, for sufficiently large ω_\parallel , the curvature of the electrode potential (8) in the z -direction may become substantial, particularly for highly excited states of out-of-plane motion. However, for a typical $\omega_\parallel/2\pi = 20$ GHz, the effective curvature-induced change of the out-of-plane field for lowest states $2m\omega_\parallel^2 r_B/e$ is only ≈ 14 V/cm.

C. Electrostatic force on helium

Electric field from the electrodes and pressure from the electrons (polaronic effect) lead to deformation of the helium surface. The effect of the electrode potential can be easily estimated by noticing that the dielectric constant of helium is close to one, $\varepsilon - 1 \approx 0.057 \ll 1$. Therefore if the surface is raised by $\xi(\mathbf{r})$, the associated change in the density (per unit area) of the free energy of helium $\Delta\mathcal{F}$ in the surface field $\mathbf{E}(\mathbf{r})$ is $-(\varepsilon - 1)E_\perp^2(\mathbf{r})\xi(\mathbf{r})/8\pi$. Bending of the surface is counteracted by surface energy, with density $\sigma(\partial\xi/\partial\mathbf{r})^2/2$, where σ is the surface tension. The competition between these two terms gives the height $\xi \sim \frac{\varepsilon-1}{8\pi} E_\perp^2 h d / \sigma$. For typical $E_\perp = 3 \times 10^2$ V/cm, $h = 0.5 \mu\text{m}$, and $d = 1 \mu\text{m}$ this gives a negligibly small $\xi < 10^{-10}$ cm. Therefore this effect can be safely ignored.

III. DECAY OF THE EXCITED ELECTRON STATE

A. The Hamiltonian of coupling to surface displacement

The major mechanism of electron relaxation for low temperatures is scattering by vibrations of the liquid helium surface. A complete calculation of the energy of coupling to surface vibrations is nontrivial. The density profile of the interface between helium and its vapor has a complicated form, with the 10%/90% interfacial width $\approx 6 - 7 \text{ \AA}$ for low temperatures [29]. As a consequence, even for a flat surface the electron potential is more complicated than the simple image potential $-\Lambda/z$ for $z > 0$ and a sharp wall at $z = 0$ (2) [26]. In particular the repulsive barrier is smooth, but it becomes high compared to the binding energy R already on the tail of the helium

density distribution. The spatial structure of surface excitations is complicated as well. However, for excitations with sufficiently long wavelengths to a good approximation the vibrating helium surface can still be considered as a corrugated infinitely high potential wall. The electron wave function is set equal to zero on the surface.

In this approximation the Hamiltonian H_i of interaction of an electron with surface vibrations is obtained by changing the electron coordinates $\mathbf{r} \rightarrow \mathbf{r}, z \rightarrow z - \xi(\mathbf{r})$ where $\xi(\mathbf{r})$ is the surface displacement, see Refs. 30, 31, 32. The interaction is a series in the ratio ξ/r_B . Typically this ratio is very small, $\sim 3 \times 10^{-3}$ for thermal displacement with characteristic wave numbers. Therefore to a good approximation H_i can be expanded in ξ , keeping only lowest-order terms. The major term, $H_i^{(1)}$, is linear in $\xi(\mathbf{r}) = \sum_{\mathbf{q}} \xi_{\mathbf{q}} e^{i\mathbf{q}\mathbf{r}}$,

$$H_i^{(1)} = \sum_{\mathbf{q}} \xi_{\mathbf{q}} e^{i\mathbf{q}\mathbf{r}} \hat{V}_{\mathbf{q}}, \quad (9)$$

with

$$\begin{aligned} \hat{V}_{\mathbf{q}} = & -\frac{i}{m}(\mathbf{q} \cdot \hat{\mathbf{p}})\hat{p}_z - \frac{i\hbar}{2m}q^2\hat{p}_z + eE_\perp + \Lambda q^2 v_{\text{pol}}(qz), \\ v_{\text{pol}}(x) = & x^{-2} [1 - xK_1(x)] \end{aligned} \quad (10)$$

Here, $\hat{\mathbf{p}} = -i\hbar\partial_{\mathbf{r}}$ is the 2D electron momentum, and $\hat{p}_z = -i\hbar\partial_z$. The first two terms in the operator $\hat{V}_{\mathbf{q}}$ describe a *kinematic* interaction, which arises because the electron wave function is set equal to zero on a non-flat surface. The term $v_{\text{pol}}(qz)$ describes the change of the polarization energy due to surface curvature [31, 32] ($K_1(x)$ is the modified Bessel function).

The quadratic in ξ coupling is

$$H_i^{(2)} = \sum_{\mathbf{q}_1, \mathbf{q}_2} \xi_{\mathbf{q}_1} \xi_{\mathbf{q}_2} \exp[i(\mathbf{q}_1 + \mathbf{q}_2)\mathbf{r}] \hat{V}_{\mathbf{q}_1 \mathbf{q}_2}. \quad (11)$$

As in the case of linear coupling, it also has kinematic [32] and polarization parts,

$$\hat{V}_{\mathbf{q}_1 \mathbf{q}_2} = \hat{V}_{\mathbf{q}_1 \mathbf{q}_2}^{(k)} + \hat{V}_{\mathbf{q}_1 \mathbf{q}_2}^{(\text{pol})}, \quad \hat{V}_{\mathbf{q}_1 \mathbf{q}_2}^{(k)} = -(\mathbf{q}_1 \mathbf{q}_2) p_z^2 / 2m, \quad (12)$$

with

$$\begin{aligned} \hat{V}_{\mathbf{q}_1 \mathbf{q}_2}^{(\text{pol})} = & -\Lambda z^{-3} [1 - u(q_1 z) - u(q_2 z) + u(|\mathbf{q}_1 + \mathbf{q}_2|z)], \\ u(x) = & x^2 K_2(x) / 2 \end{aligned} \quad (13)$$

1. Coupling to ripplons

The biggest contribution to surface vibrations comes from capillary waves, ripplons. The displacement $\xi_{\mathbf{q}}$ is related to the creation and annihilation operators of ripplons by

$$\xi_{\mathbf{q}} = S^{-1/2} (\hbar q / 2\rho\omega_q)^{1/2} (b_{\mathbf{q}} + b_{-\mathbf{q}}^\dagger),$$

where S is the area of the system, ρ is the helium density, and the ripplon frequency $\omega_q = (\sigma q^3 / \rho)^{1/2}$ for $q \gg (\rho g / \sigma)^{1/2}$.

The change of variables used to take into account the hard wall potential on helium surface leads also to extra terms in the kinetic energy of ripples coupled to the electron, which is yet another source of electron-ripple coupling [32]. Compared to similar terms in Eqs. (9), (11), these terms have an extra parameter $\omega_q m / \hbar q^2$, which is extremely small for typical q .

There are several limitations on the wave numbers q of ripples for which the electron-ripple coupling has the form (9), (11). Monarkha and Shikin [32] argue that essentially qr_B should be $\lesssim 1$. Clearly, q should be small compared to the reciprocal width of the helium liquid-vapor interface and the reciprocal decay length of the electron wave function into helium (note that there is no factor 2π here, because a capillary wave with wave number \mathbf{q} decays into helium as $\exp(qz)$, for a sharp interface). Both lengths are of order of a few angstroms, which means that the large- q cutoff q_{\max} should be $\lesssim 10^7 \text{ cm}^{-1}$.

A cutoff at 10^7 cm^{-1} is consistent also with the condition that $H_i^{(2)}$ (11) be small. To first order in the kinematic part of $H_i^{(2)}$, which dominates for large q , the relative change of the electron kinetic energy for motion transverse to the surface for $T = 0$ is

$$\delta K/K = \hbar q_{\max}^{7/2} / 14\pi(\sigma\rho)^{1/2}.$$

This gives $\delta K/K \approx 3 \times 10^{-4}$ for $q_{\max} = 10^7 \text{ cm}^{-1}$ (for $q_{\max} = 10^8 \text{ cm}^{-1}$ the correction would be equal to 1). Presumably the interaction with ripples as a whole and in particular inelastic scattering by ripples falls down for q much bigger than 10^7 cm^{-1} , because for such momentum transfer an electron “resolves” atomic structure of helium. Finding H_i for such q requires a full calculation of the ripple-induced modulation of the electron potential for the diffuse helium surface, which is not the subject of the present paper.

In what follows we will use spectroscopic notations and evaluate the decay rate as $\Gamma = 1/2T_1$, where T_1 is the lifetime of the excited state. Defined in this way, Γ gives the decay rate of the off-diagonal matrix element ρ_{12} of the electron density matrix and the decay-induced broadening of the absorption line.

B. One-ripple decay

The important consequence of strong in-plane confinement is that it essentially eliminates decay processes in which an electron transition is accompanied by emission or absorption of a ripple. This happens because ripples are very slow, and energy conservation in a transition requires transfer of too large momentum for an electron to accommodate.

For low temperatures, $k_B T \ll \hbar\omega_{\parallel}$, qubit relaxation is due to electron transitions $|2, 0, 0\rangle \rightarrow |1, \nu, m_{\nu}\rangle$ from the ground vibrational level of the state $|2\rangle$ of z -motion into excited states of in-plane vibrations in the state $|1\rangle$ of z -motion, see Fig. 2. Minimal energy transfer is of the

order of the vibrational level spacing $\hbar\omega_{\parallel}$. It corresponds to a transition into vibrational states with the energy closest to E_2 from below, i.e. with $\nu = \nu_c \equiv \text{int}[(E_2 - E_1)/\hbar\omega_{\parallel}]$. The squared matrix element of the transition $|\langle \nu = m_{\nu} = 0 | \exp(i\mathbf{q}\mathbf{r}) | \nu_c, m_{\nu_c} \rangle|^2$ is exponentially small for $q \gg \nu_c^{1/2}/a_{\parallel}$, where

$$a_{\parallel} = (\hbar/m\omega_{\parallel})^{1/2} \quad (14)$$

is the electron in-plane localization length.

The frequency of ripples with $q = \nu_c^{1/2}/a_{\parallel}$ is much less than ω_{\parallel} provided

$$\omega_{\parallel} \gg (\sigma/\rho)^{1/2} [m(E_2 - E_1)/\hbar^2]^{3/4}.$$

This inequality is satisfied already for $\omega_{\parallel}/2\pi \gtrsim 0.2 \text{ GHz}$, whereas a typical ω_{\parallel} for confined electrons is $\sim 20 \text{ GHz}$. Therefore one-ripple decay is exponentially improbable. This result does not change for a many-electron system provided the bands of in-plane vibrations are narrow, as discussed in Sec. II B, see Eq. (6).

C. Two-ripple decay

Even for large separation between electron energy levels, where one-ripple decay processes are exponentially suppressed by the restriction on the transferred momentum, decay into two ripples may still be possible [34, 35]. Indeed, each of the wave vectors $\mathbf{q}_1, \mathbf{q}_2$ of the participating ripples can be big, this is only their sum that is limited by the typical reciprocal electron wavelength. The energy and momentum conservation law require than that the ripples have nearly same frequencies and propagate in opposite directions, $\mathbf{q}_1 \approx -\mathbf{q}_2$ and $\omega_{q_1} \approx \omega_{q_2} \approx \delta E/2\hbar$, where δE is the change of the electron energy.

A typical minimal value of δE for the decay of the electron state $|2\rangle$ is determined by the distance between the energy levels of in-plane vibrations $\hbar\omega_{\parallel}$. The ripple frequency $\omega_q/2\pi$ becomes equal to typical $\omega_{\parallel}/4\pi = 10 \text{ GHz}$ for $q = 1.2 \times 10^7 \text{ cm}^{-1}$, i.e. presumably beyond the range of applicability of the electron-ripple coupling theory (9), (11). Therefore we use this theory to estimate the rate of decay only with minimal energy transfer, i.e. we are interested in ripple-induced transitions $|2, 0, 0\rangle \rightarrow |1, \nu, m_{\nu}\rangle$ with $\nu = \nu_c$. In this case

$$\delta E = E_2 - E_1 - \nu_c \hbar\omega_{\parallel}.$$

In calculating the total rate of decay into different states of the ν th vibrational energy level of a two-dimensional oscillator it is convenient to use the relation

$$\begin{aligned} g(\nu, q) &= \sum_{m_{\nu}} |\langle j, 0, 0 | e^{i\mathbf{q}\mathbf{r}} | j, \nu, m_{\nu} \rangle|^2 \\ &= x^{\nu} e^{-x} / \nu!, \quad x = q^2 a_{\parallel}^2 / 2 \end{aligned} \quad (15)$$

independent of $j = 1, 2$.

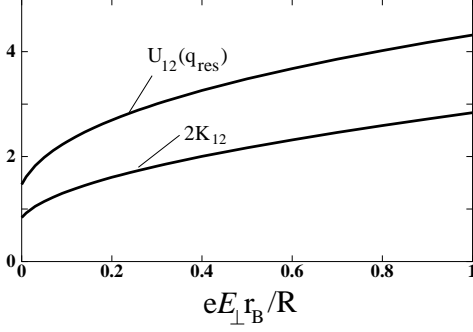


FIG. 4: Scaling factors K_{12} (16) and $U_{12}(q)$ (17) in the estimated probabilities of scattering into two ripples due to the kinematic and polarization couplings, respectively. The ripples propagate in opposite directions with nearly same wave numbers q_{res} given by the energy conservation condition $2\omega_q = \delta E/\hbar$ for $q = q_{\text{res}}$. Only transitions with smallest energy transfer δE are taken into account and the approximation of an infinite sharp potential wall for an electron on helium surface is used. The data for U_{12} refer to $q_{\text{res}} = 3.5/r_B$, which corresponds to $\delta E/2\pi\hbar \approx 5$ GHz.

For the kinematic two-ripple coupling, which is given by Eq. (11) with $\hat{V}_{\mathbf{q}_1\mathbf{q}_2} = \hat{V}_{\mathbf{q}_1\mathbf{q}_2}^{(k)}$, the decay rate $\Gamma_{2r}^{(k)}$ with account taken of (15) is

$$\Gamma_{2r}^{(k)} = \frac{K_{12}^2 R^2 q_{\text{res}}^{7/2}}{24\pi a^2 \rho^{1/2} \sigma^{3/2}}, \quad K_{12} = \frac{\langle 1 | p_z^2 / 2m | 2 \rangle}{R}. \quad (16)$$

Here, q_{res} is the ripple wave vector given by the energy conservation law, $\omega_{q_{\text{res}}} = \delta E/2\hbar$, and we assumed that $q_{\text{res}} \gg \nu_c^{1/2}/a_{\parallel}$, which is the condition for the ripples created in the transition to propagate in opposite directions. The scaled matrix element of the kinetic energy K_{12} is shown in Fig. 4.

The rate $\Gamma_{2r}^{(k)}$ depends on q_{res} and therefore on δE very steeply, $\Gamma_{2r}^{(k)} \propto \delta E^{7/3}$. For $\delta E = \hbar\omega_{\parallel}/4$ and $\omega_{\parallel}/2\pi = 20$ GHz we have $q_{\text{res}} \approx 4.6 \times 10^6 \text{ cm}^{-1}$ and $\Gamma_{2r}^{(k)} = 7.6 \times 10^2 - 3.8 \times 10^3 \text{ s}^{-1}$ for the pressing field $E_{\perp} = 0 - 300 \text{ V/cm}$. This value can be decreased by reducing δE . However, Eq. (16) is probably an overestimate even for the δE used above, because it is based on the approximation of an infinite-wall potential for an electron and the assumptions that the helium surface is sharp.

The expression for the two-ripple decay rate $\Gamma_{2r}^{(\text{pol})}$ due to the polarization two-ripple interaction (13) has the same form as Eq. (16). Just the factor $K_{12}^2 q_{\text{res}}^{7/2}$ in Eq. (16) has to be replaced with $U_{12}^2(q_{\text{res}})/r_B^4 q_{\text{res}}^{1/2}$, where U_{12} is determined by the matrix element of $2r_B^3 \hat{V}_{\mathbf{q}_1\mathbf{q}_2}^{(\text{pol})}/\Lambda$ (13) on the functions $|1\rangle, |2\rangle$. The major contribution to this matrix element comes from the range of comparatively small z , and therefore for an estimate one can re-

place $K_2(|\mathbf{q}_1 + \mathbf{q}_2|z)$ with its small- z limit in (13). Then

$$U_{12}(q) = 2r_B^3 \langle 1 | z^{-3} [2 - q^2 z^2 K_2(qz)] | 2 \rangle. \quad (17)$$

The coefficient U_{12} as given by Eq. (17) is shown in Fig. 4. For δE and ω_{\parallel} chosen above we have $\Gamma_{2r}^{(\text{pol})}/\Gamma_{2r}^{(k)} \sim 0.1$ for $E_{\perp} = 0 - 300 \text{ V/cm}$. The rate $\Gamma_{2r}^{(\text{pol})}$ grows much slower than $\Gamma_{2r}^{(k)}$ with increasing q_{res} (and thus with increasing δE).

Besides the terms $\Gamma_{2r}^{(k)}$ and $\Gamma_{2r}^{(\text{pol})}$ due to purely kinematic and polarization mechanisms, there is a contribution to the decay rate from the interference of these two mechanisms. It is smaller than $\Gamma_{2r}^{(k)} + \Gamma_{2r}^{(\text{pol})}$ and will not be discussed.

D. Phonon-induced decay

An important channel of inelastic electron scattering is decay into phonons in helium. For a typical energy transfer $\delta E \sim \hbar\omega_{\parallel}$, the wave numbers of the phonons participating in the decay are $\sim \omega_{\parallel}/v_s$ (v_s is the sound velocity in helium). On the other hand, the in-plane momentum transfer is limited to $\sim \hbar/a_{\parallel} \ll \hbar\omega_{\parallel}/v_s$. As a result, only phonons propagating nearly normal to the surface (in the z -direction) may be excited in a one-phonon decay (cf. Ref. 34).

1. Decay due to phonon-induced surface displacement

Two coupling mechanisms are important for decay into phonons. One is related to phonon-induced displacement of the helium surface. This mechanism can be quantitatively described in the approximation of a sharp helium boundary, which provides an infinitely high potential barrier for electrons. The coupling is given by Eqs. (9), (10) with $\xi_{\mathbf{q}}$ being a phonon-induced component of the surface displacement. As in the case of coupling to ripples, it would be unreasonable to use it for short-wavelength phonons, in particular for phonons with $q_z \gg 10^7 \text{ cm}^{-1}$. For typical $\omega_{\parallel}/2\pi = 20$ GHz we have $q_z \sim \omega_{\parallel}/v_s \sim 5 \times 10^6 \text{ cm}^{-1}$. Therefore we will again consider decay of the state $|2, 0, 0\rangle$ into closest lower-energy states $|1, \nu, m_{\nu}\rangle$.

For typical $\mathbf{q} \equiv (q_x, q_y) \sim 1/a_{\parallel}$ and $q_z \lesssim \omega_{\parallel}/v_s$ we have $\sigma q^2/\rho v_s^2 q_z \ll 1$. This inequality allows one to think of helium surface as a free boundary for phonons and to ignore coupling between phonons and ripples [36, 37]. Then surface displacement is simply related to the Fourier components $u_{\mathbf{Q}}$ of the phonon displacement field [here, $\mathbf{Q} = (\mathbf{q}, q_z)$ is the 3D phonon wave vector, and $u_{\mathbf{Q}}$ is the displacement along \mathbf{Q}]. In turn, $u_{\mathbf{Q}}$ is related to the operators of creation and annihilation of phonons in a standard way,

$$u_{\mathbf{Q}} = (\hbar/2\rho V v_s Q)^{1/2} (c_{\mathbf{Q}} - c_{-\mathbf{Q}}^{\dagger}) \quad (18)$$

(V is the volume of helium).

With (18), we obtain the rate of decay $|2, 0, 0\rangle \rightarrow |1, \nu_c, m_\nu\rangle$ due to phonon-induced surface displacement $\Gamma_{\text{ph}}^{(s)}$ in the form

$$\Gamma_{\text{ph}}^{(s)} = (8\pi^2 \rho v_s \delta E)^{-1} \times \sum_{m_\nu=0}^{\nu_c} \int d\mathbf{q} |\langle 2, 0, 0 | e^{i\mathbf{q}\mathbf{r}} \hat{V}_{\mathbf{q}} | 1, \nu_c, m_\nu \rangle|^2. \quad (19)$$

We start with the contribution to $\Gamma_{\text{ph}}^{(s)}$ from the kinematic terms in $\hat{V}_{\mathbf{q}}$ [the first two terms in Eq. (10)]. Taking into account that the diagonal with respect to out-of-plane motion matrix element

$$\begin{aligned} & \langle j, 0, 0 | \exp(i\mathbf{q}\mathbf{r}) [(\mathbf{q}\hat{\mathbf{p}}) + \hbar q^2/2] | j, \nu, m_\nu \rangle \\ &= -\nu m \omega_{\parallel} \langle j, 0, 0 | \exp(i\mathbf{q}\mathbf{r}) | j, \nu, m_\nu \rangle \quad (j = 1, 2) \end{aligned}$$

and using Eq. (15), we obtain for the kinematic contribution

$$\Gamma_{\text{ph}}^{(s;k)} \approx (E_2 - E_1)^2 z_{12}^2 \frac{\nu_c^2 m^3 \omega_{\parallel}^3}{4\pi \rho v_s \hbar^3 \delta E}. \quad (20)$$

The numerical value of $\Gamma_{\text{ph}}^{(s;k)}$ is $7.8 \times 10^2 \text{ s}^{-1}$ for $E_{\perp} = 0$, $\omega_{\parallel}/2\pi = 21.1 \text{ GHz}$, and $\delta E \approx \hbar \omega_{\parallel}$ ($\nu_c = 5$ in this case). It goes up to $\sim 1.5 \times 10^4 \text{ s}^{-1}$ for $E_{\perp} = 300 \text{ V/cm}$ and $\omega_{\parallel}/2\pi = 20.6 \text{ GHz}$ (in this case $\nu_c = 12$). The values of ω_{\parallel} were adjusted here to meet the condition $\delta E = E_2 - E_1 - \nu_c \hbar \omega_{\parallel} \approx \hbar \omega_{\parallel}$ for the energy spectrum calculated for a sharp helium boundary; the real level spacing is a few percent smaller [24, 26, 27], leading to a slightly smaller $\Gamma_{\text{ph}}^{(s;k)}$ for $\omega_{\parallel}/2\pi \sim 20 \text{ GHz}$. We expect a more significant change (reduction) of $\Gamma_{\text{ph}}^{(s;k)}$ due to diffuseness of helium surface.

The contribution to $\Gamma_{\text{ph}}^{(s)}$ from the polarization term in $\hat{V}_{\mathbf{q}}$ [the last term in Eq. (10)] has the form

$$\Gamma_{\text{ph}}^{(s;\text{pol})} \approx \frac{4R^2 r_B^2}{\nu_c! \pi \rho v_s \delta E a_{\parallel}^6} \int_0^\infty dx e^{-x} x^{\nu_c+2} v^2(x), \quad (21)$$

where $v^2(x) = |\langle 1 | v_{\text{pol}}[(2x)^{1/2} z/a_{\parallel}] | 2 \rangle|^2$. The numerical value of $\Gamma_{\text{ph}}^{(s;\text{pol})}$ is $\sim 7 \times 10^2 \text{ s}^{-1}$ for $E_{\perp} = 0$ and goes up to $\sim 7 \times 10^3 \text{ s}^{-1}$ for $E_{\perp} = 300 \text{ V/cm}$ (we used same ω_{\parallel} as in the above estimate of $\Gamma_{\text{ph}}^{(s;k)}$).

There exists also a contribution to $\Gamma_{\text{ph}}^{(s)}$ (19) from the interference term, which is bilinear in the polarization and kinematic interaction energies (10) (the terms $\Gamma_{\text{ph}}^{(s;k,\text{pol})}$ are quadratic in these interactions). It can be obtained from (19) in the same way as $\Gamma_{\text{ph}}^{(s;k,\text{pol})}$. It is positive and of the same order of magnitude as $\Gamma_{\text{ph}}^{(s;k,\text{pol})}$.

The scattering rate $\Gamma_{\text{ph}}^{(s)}$ can be reduced by decreasing the pressing field E_{\perp} . More importantly, it can also be

reduced by increasing the frequency ω_{\parallel} , in which case the wavelength of the phonons to which the energy is transferred will become smaller than the width of the diffusive layer on helium surface (in fact, the above calculation probably already overestimates the scattering rate). A transition to such frequency can be accomplished with a magnetic field applied transverse to the surface, as initially suggested in Ref. 15.

2. Decay due to phonon-induced modulation of the helium dielectric constant

Another mechanism of coupling to phonons is through phonon-induced modulation of the image potential of an electron. It results from the modulation of the helium density $\delta\rho$ and related modulation of the dielectric constant $\delta\epsilon$. It is reasonable to assume that, for long wavelength phonons, $\delta\epsilon = (\epsilon - 1)\delta\rho/\rho$. To lowest order in $\epsilon - 1, \delta\epsilon$ the coupling energy is

$$H_i^{(d)} = -\frac{1}{8\pi} \int d\mathbf{R}' \delta\epsilon(\mathbf{R}') E^2(\mathbf{R}'; \mathbf{R}).$$

Here the integration goes over the space occupied by helium, $\mathbf{R} \equiv (\mathbf{r}, z)$ is the 3D position vector, and $\mathbf{E}(\mathbf{R}'; \mathbf{R})$ is the electric field at \mathbf{R}' created by an electron located at a point \mathbf{R} .

The coupling Hamiltonian can be written in the form

$$H_i^{(d)} = \sum_{\mathbf{Q}} u_{\mathbf{Q}} \exp(i\mathbf{q}\mathbf{r}) \hat{V}_{\mathbf{Q}}^{(d)}, \quad \hat{V}_{\mathbf{Q}}^{(d)} = i\Lambda q Q v^{(d)} \quad (22)$$

with $v^{(d)} \equiv v^{(d)}(q, q_z, z)$ being

$$v^{(d)} = \int_0^\infty dz' (z + z')^{-1} e^{-iq_z z'} K_1[q(z + z')]. \quad (23)$$

As in the case discussed in the previous section, the coupling (22) gives rise to phonon-induced electron transitions between electron energy levels accompanied by emission of a phonon. Here, too, typical in-plane wave numbers of emitted phonons q are much less than the normal to the surface wave number $q_z \approx \delta E/\hbar u$. The expression for the corresponding decay rate $\Gamma_{\text{ph}}^{(d)}$ has the form

$$\Gamma_{\text{ph}}^{(d)} \approx \frac{R^2 \delta E r_B^2}{\pi \hbar^2 \rho v_s^3} \int_0^\infty dq q^3 |\langle 2 | v^{(d)} | 1 \rangle|^2 g(\nu_c, q) \quad (24)$$

Evaluation of the integral is largely simplified by the fact that the function $q^3 g(\nu, q)$ sharply peaks at $q = q_\nu \approx (2\nu + 3)^{1/2}/a_{\parallel}$. Therefore, with an error less than 10% one can replace $v^{(d)}$ in (24) by its value (23) for $q = q_\nu$.

For $\omega_{\parallel}/2\pi = 20 \text{ GHz}$ and $\delta E = \hbar \omega_{\parallel}$, the value of $\Gamma_{\text{ph}}^{(d)}$ varies from $\sim 1 \times 10^4 \text{ s}^{-1}$ to $\sim 6 \times 10^4 \text{ s}^{-1}$ with E_{\perp} increasing from 0 to 300 V/cm. However, these values have to be taken with care. The integrand in $v^{(d)}$ (23) is a fast oscillating function of z' on the characteristic scale

$z' \sim r_B$, because typically $q_z r_B \gg 1$ ($q_z r_B \approx 4$ for chosen ω_{\parallel}). In addition, the matrix element of $v^{(d)}$ in (24) has an integrable singularity for $z = z' = 0$ (the wave functions $\psi_n(z) \propto z$ for $z \rightarrow 0$). As a result, a significant contribution to the matrix element comes from small distances from the helium surface, $z' \ll r_B$. Changing, in view of diffuseness of helium surface, the limit of integration in (23) from $z' = 0$ to a more reasonable $z' = r_B/10$ reduces the value of $\Gamma_{\text{ph}}^{(d)}$ by a factor of 3.

The decay rate $\Gamma_{\text{ph}}^{(d)}$ decreases with the increasing δE roughly as $1/\delta E$ (and even faster, in view of the “dead” layer on the diffuse surface). For higher δE and, respectively, for higher wave numbers of resonant phonons, the simple approximation (22) no longer describes the electron-phonon interaction. Therefore, as in the case of scattering due to phonon-induced surface deformation, a way to reduce the scattering rate is to increase the frequency of in-plane vibrations.

Full coupling to phonons is given by the sum of all couplings discussed in this section, with $\hat{V}_{\mathbf{q}}$ in Eq. (19) replaced by $\hat{V}_{\mathbf{q}} + \alpha_{\mathbf{Q}} \hat{V}_{\mathbf{Q}}^{(d)}$ with $\alpha_{\mathbf{Q}} \approx 1$ for typical \mathbf{Q} . The total rate of scattering by phonons contains cross-terms which describe interference of different coupling mechanisms. As mentioned above, we omit these terms, because they do not change the overall estimate of the rate. We note that an interesting situation may occur if one of the transition frequencies of the electron comes in resonance with the roton energy. In this case we expect an increase of the decay rate. Observing it would be a direct demonstration of coupling to volume excitations in helium.

IV. DEPHASING DUE TO RIPPLON SCATTERING

In addition to depopulation of the excited state of a qubit, electron coupling to excitations in liquid helium leads also to decoherence or dephasing, i.e. to decay of

the phase difference between the qubit states $|2, 0, 0\rangle$ and $|1, 0, 0\rangle$. The mechanism of this decay is random modulation, by thermal fluctuations in helium, of the distance between the energy levels 1 and 2. In other terms it can be described as quasi-elastic scattering of thermal excitations off an electron. The scattering is different in different electron states. Therefore it randomizes the phase difference between the wave functions of the states without causing interstate transitions. The corresponding mechanism is known for defects in solids [33] as modulational or Raman broadening. For electrons on helium it was discussed in Refs. 15, 34.

Dephasing comes primarily from coupling to ripples, because these excitations are soft. A typical wave number q_r and frequency ω_r of ripples coupled to an electron are given by

$$q_r = 1/a_{\parallel}, \quad \omega_r \equiv \omega_{q_r} = (\sigma/\rho)^{1/2} q_r^{3/2}. \quad (25)$$

For $\omega_{\parallel}/2\pi = 20$ GHz we have $\omega_r/2\pi \approx 4.8 \times 10^7$ Hz ≈ 2.3 mK. Therefore even for temperatures as low as 10 mK ripplon occupation numbers are large. To the lowest order of perturbation theory, quasi-elastic ripplon scattering by an electron is determined by two-ripplon coupling, with the Hamiltonian

$$H_i^{(\text{qe})} = \sum_{j=1,2} \sum_{\mathbf{q}, \mathbf{q}'} v_{\mathbf{q}\mathbf{q}'} b_{\mathbf{q}}^{\dagger} b_{\mathbf{q}'} |j, 0, 0\rangle \langle j, 0, 0|. \quad (26)$$

Individual terms in the sum over \mathbf{q}, \mathbf{q}' describe scattering of a ripplon with wave number \mathbf{q}' into a ripplon with wave number \mathbf{q} . The momentum is transferred to the electron, and no transitions between electron states occur. We will consider terms with $\mathbf{q} \neq \mathbf{q}'$; the term with $\mathbf{q} = \mathbf{q}'$ gives the shift of the electron energy levels.

The matrix elements $v_{\mathbf{q}\mathbf{q}'} j$ are linear in the parameters of the direct two-ripplon coupling $H_i^{(2)}$ (11) and quadratic in the parameters of the one-ripplon coupling $H_i^{(1)}$ (9),

$$v_{\mathbf{q}\mathbf{q}'} j \approx \frac{\hbar(qq')^{1/2}}{S\rho(\omega_q\omega_{q'})^{1/2}} \left[\langle j, 0, 0 | \hat{V}_{-\mathbf{q}, \mathbf{q}'} | j, 0, 0 \rangle e^{-(\mathbf{q}-\mathbf{q}')^2 a_{\parallel}^2/4} - \sum_{\nu, m_{\nu}} \left(\mathcal{V}_{\mathbf{q}\mathbf{q}'}^{j\nu m_{\nu}} + \mathcal{V}_{-\mathbf{q}'-\mathbf{q}}^{j\nu m_{\nu}} \right) (\hbar\nu\omega_{\parallel})^{-1} \right] \quad (27)$$

where $\mathcal{V}_{\mathbf{q}\mathbf{q}'}^{j\nu m_{\nu}} = V_{\mathbf{q}}^{j\nu m_{\nu}} \left(V_{\mathbf{q}'}^{j\nu m_{\nu}} \right)^*$ and $V_{\mathbf{q}}^{j\nu m_{\nu}} = \langle j, 0, 0 | \hat{V}_{-\mathbf{q}} e^{-i\mathbf{q}\mathbf{r}} | j, \nu, m_{\nu} \rangle$. In calculating renormalization of the parameters $v_{\mathbf{q}\mathbf{q}'} j$ due to one-ripplon coupling we disregarded the contribution from virtual transitions into different states of out-of-plane motion $|j'\rangle$, because they involve a large energy change (it is straightforward to incorporate the corresponding terms). We also disregarded ripplon energies $\hbar\omega_q$ compared to $\hbar\omega_{\parallel}$.

A calculation similar to that for crystal lattice defects

[33] gives the phase relaxation rate Γ_{ϕ} for the coupling (26) in the form

$$\Gamma_{\phi} = \frac{\pi}{\hbar^2} \sum_{\mathbf{q}, \mathbf{q}'} |v_{\mathbf{q}\mathbf{q}'} 1 - v_{\mathbf{q}\mathbf{q}'} 2|^2 \times \bar{n}(\omega_{\mathbf{q}}) [\bar{n}(\omega_{\mathbf{q}'} + 1) \delta(\omega_{\mathbf{q}} - \omega_{\mathbf{q}'}), \quad (28)$$

where $\bar{n}(\omega) = [\exp(\hbar\omega/k_B T) - 1]^{-1}$ is the Planck number. It follows from Eq. (28) that only thermally excited ripples with $\omega_q \lesssim k_B T/\hbar$ contribute to the rate Γ_{ϕ} . In

what follows we will estimate contributions to Γ_ϕ from different mechanisms of electron-ripplon coupling taken separately and will again ignore cross-terms, which contain products of coupling constants for different mechanisms.

The contribution to the phase relaxation rate $\Gamma_\phi^{(k)}$ from the direct two-ripplon kinematic coupling (12) has a simple form in the case where the frequencies of ripples with $q \lesssim 1/a_\parallel$ are small compared to $k_B T/\hbar$. Then $\Gamma_\phi^{(k)}$ is determined primarily by forward scattering of ripples off the electron, with $|\mathbf{q} - \mathbf{q}'| \lesssim 1/a_\parallel$, but with $\omega_q = \omega_{q'} \sim k_B T/\hbar \gg \omega_r$. Calculating the integral over the angle between \mathbf{q} and \mathbf{q}' by the steepest descent method, we obtain

$$\Gamma_\phi^{(k)} = \frac{\pi^{1/2} \rho}{27\sqrt{2}a_\parallel} \left(\frac{k_B T}{\hbar \sigma} \right)^3 R^2 \tilde{K}_{12}^2, \quad (29)$$

where \tilde{K}_{12} is the difference of the expectation values of the kinetic energy $p_z^2/2m$ in the states 1 and 2 divided by R ; we have $\tilde{K}_{12} = 3/4$ for $E_\perp = 0$, and \tilde{K}_{12} decreases with increasing E_\perp . The numerical value of $\Gamma_\phi^{(k)}$ is very small for low temperatures, $\Gamma_\phi^{(k)} \lesssim 0.7 \times 10^2 \text{ s}^{-1}$ for $T=10$ mK and $\omega_\parallel/2\pi = 20$ GHz.

The contribution from the direct two-ripplon polarization coupling (13) can be estimated by utilizing the fact that the wave vectors of thermal ripples $q_T = (\rho/\sigma)^{1/3} (k_B T/\hbar)^{2/3}$ are less than $1/r_B$ for low temperatures. To lowest order in $q_T r_B$ the polarization contribution is again given by Eq. (29), but now \tilde{K}_{12} is the difference of the expectation values of the potential energy $\Lambda/2z$ divided by R . The corresponding rate is of the same order as $\Gamma_\phi^{(k)}$.

We now estimate the phase relaxation rate due to one-ripplon coupling (10). We note first that the kinematic terms in (10) drop out of the matrix elements $v_{\mathbf{q}\mathbf{q}'j}$, because they do not have diagonal matrix elements on the functions $|j, 0, 0\rangle$ ($j = 1, 2$). The terms quadratic in the electric field E_\perp drop out from the difference $v_{\mathbf{q}\mathbf{q}'1} - v_{\mathbf{q}\mathbf{q}'2}$, because they are independent of the electron state normal to the surface. The major contribution therefore comes from the polarization one-ripplon coupling $\propto v_{\text{pol}}$ in $\hat{V}_{\mathbf{q}}$ (10). We will denote it as $\Gamma_\phi^{(\text{pol})}$.

Polarization terms in the operators $\hat{V}_{\mathbf{q}}$ do not depend on the in-plane electron coordinate. This makes it possible to calculate the sum over ν, m_ν in Eq. (27) for $v_{\mathbf{q}\mathbf{q}'j}$. The calculation is simplified in the case $k_B T \gg \omega_r$ where $q \gg 1/a_\parallel$ and $\mathbf{q} \cdot \mathbf{q}' \approx qq' \gg a_\parallel^{-2}$. Then the sum of $\mathcal{V}_{\mathbf{q}\mathbf{q}'}^{j\nu m_\nu}/\hbar\nu\omega_\parallel$ can be approximated by

$$2\langle j|\hat{V}_{-\mathbf{q}}|j\rangle\langle j|\hat{V}_{\mathbf{q}'}|j\rangle \exp[-(\mathbf{q} - \mathbf{q}')^2 a_\parallel^2/4] (\hbar\omega_\parallel a_\parallel^2 qq')^{-1}.$$

In this approximation we obtain

$$\Gamma_\phi^{(\text{pol})} \sim \frac{\rho}{a_\parallel} \left(\frac{k_B T}{\hbar \sigma} \right)^3 R^2 k_{12}^2. \quad (30)$$

Here we assumed that the coefficient $k_{12} = |\langle 1|v_{\text{pol}}(qz)|1\rangle|^2 - |\langle 2|v_{\text{pol}}(qz)|2\rangle|^2$ is a smooth function of q for actual $q \sim q_T$. Its numerical value is ~ 0.23 for $q \approx q_T$ and $T=10$ mK, it weakly depends on the pressing field E_\perp . The phase relaxation rate is $\Gamma_\phi^{(\text{pol})} \sim 10^2 \text{ s}^{-1}$. The one-ripplon polarization coupling is therefore a major mechanism of phase relaxation for a confined electron.

The overall ripplon-induced phase relaxation rate appears to be small. It displays an unusual temperature dependence T^3 , and comparatively weakly depends on the in-plane frequency ω_\parallel . We note that it is much less than our previous estimate [15] obtained for the case of in-plane confinement by a magnetic field.

V. RIPPLON-INDUCED SIDEBAND ABSORPTION

An important consequence of coupling to ripples is the occurrence of sidebands in the spectrum of microwave absorption by a confined electron. Sidebands are formed by an electron $|1, 0, 0\rangle \rightarrow |2, 0, 0\rangle$ transition accompanied by creation or annihilation of one or several ripples. Ripplon sidebands for a confined electron are similar to phonon sidebands in absorption spectra of defects in solids [33]. They can be understood from the Franck-Condon picture of an electron transition as happening for an instantaneous ripplon configuration. Since equilibrium ripplon positions are different in the ground and excited electron states, the transition is accompanied by excitation or absorption of ripples, and the transition energy differs from its value $E_2 - E_1$ in the absence of coupling to ripples.

In order to describe the effect it suffices to keep only diagonal in the relevant electron states $|j, 0, 0\rangle$ part of the Hamiltonian of electron-ripplon coupling. One can then apply a standard canonical transformation which shifts ripplon coordinates so that they are counted off from their equilibrium values in the ground electron state. The transformed one-ripplon interaction Hamiltonian (9), (10) then takes a Franck-Condon form

$$H_i^{\text{FC}} = \sum_{\mathbf{q}} \xi_{\mathbf{q}} \Lambda F(q) |2, 0, 0\rangle \langle 2, 0, 0|, \quad (31)$$

$$F(q) = q^2 [\langle 2|v_{\text{pol}}(qz)|2\rangle - \langle 1|v_{\text{pol}}(qz)|1\rangle] e^{-q^2 a_\parallel^2/4}.$$

For weak coupling, of primary interest are one-ripplon sidebands. Because ripplon occupation numbers are big for $k_B T \gg \hbar\omega_r$, the absorption cross-sections for electron transitions accompanied by absorption and emission of a ripplon are the same. Respectively, the sidebands are symmetrical as functions of frequency detuning $\Delta\omega = \omega - (E_2 - E_1)/\hbar$ (we have $|\Delta\omega| \sim \omega_r \ll (E_2 - E_1)/\hbar$). The absorption is quadratic in the electron-ripplon coupling parameters and can be calculated by perturbation theory in H_i^{FC} . From (31) we obtain for the scaled sideband

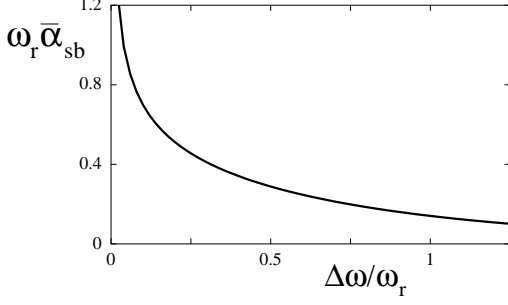


FIG. 5: Scaled absorption coefficient in the sideband $\bar{\alpha}_{\text{sb}}$ (32) vs. frequency detuning $\Delta\omega = \omega - (E_2 - E_1)/\hbar$ for $E_{\perp} = 0$ and $\omega_{\parallel}/2\pi = 20$ GHz.

absorption coefficient $\alpha_{\text{sb}}(\omega)$

$$\alpha_{\text{sb}}(\omega) = G_{\text{sb}} \bar{\alpha}_{\text{sb}}(\omega), \quad G_{\text{sb}} = \frac{k_B T R^2 r_B^2 \rho}{\pi \hbar^2 \sigma^2 a_{\parallel}},$$

$$\bar{\alpha}_{\text{sb}} = a_{\parallel} \int dq q^{-4} F^2(q) \delta(\Delta\omega \pm \omega_q). \quad (32)$$

The full absorption coefficient is given by α_{sb} multiplied by the integral over frequency of the zero-ripplon absorption coefficient. The halfwidth of the zero-ripplon line Γ is the sum of the decay and dephasing rates calculated above. In (32) we assumed that $|\Delta\omega| \gg \Gamma$; this inequality is well satisfied in the interesting region $|\Delta\omega| \sim \omega_r$, since from the above estimates $\omega_r/\Gamma \gtrsim 10^4$.

The intensity of the sideband is determined by the factor G_{sb} . For $T=10$ mK and $\omega_{\parallel}/2\pi = 20$ GHz we have $G_{\text{sb}} \approx 0.1$. The smallness of G_{sb} indicates that sidebands formed by two- or many-ripplon processes are not important.

The scaled absorption coefficient in the one-ripplon sideband is shown in Fig. 5. It monotonically decreases with the increasing distance $|\Delta\omega|$ from the zero-ripplon line. For small $|\Delta\omega|$ (but $|\Delta\omega| \gg \Gamma$) we have $\bar{\alpha}_{\text{sb}} \propto |\Delta\omega|^{-1/3}$. As expected, decay of the sideband with increasing $|\Delta\omega|$ is much slower than decay of the Lorentzian tail of the zero-ripplon line $\propto \Gamma/(\Delta\omega)^2$. For large $|\Delta\omega|/\omega_r$, the sideband absorption falls off as $\exp[-(|\Delta\omega|/\omega_r)^{4/3}/2]$, because coupling to short-wavelength ripples is exponentially weak. We note that the one-ripplon sidebands do not display structure, in contrast to sidebands in electron-phonon systems in solids that reflect singularities in the phonon density of states.

A. Intensity of the zero-ripplon line

The integral intensity of the electron absorption spectrum (integral over frequency of the absorption coefficient) is determined by the matrix element of the dipolar transition $\propto z_{12}$ and is independent of the electron-

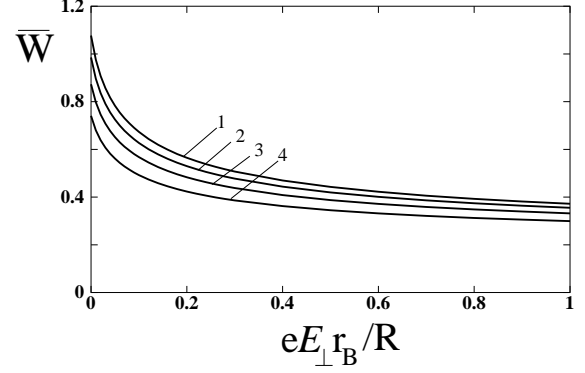


FIG. 6: Scaling factor \bar{W} in the expression (33) for the Debye-Waller exponent W . The curves 1 to 4 refer to $r_B/a_{\parallel} = 0.18, 0.25, 0.35, 0.5$ ($\omega_{\parallel}/2\pi \approx 10, 20, 39, 79$ GHz, respectively).

ripplon coupling for $E_2 - E_1 \gg \hbar\omega_r$. However, the intensity of the zero-ripplon line is reduced, because of the sidebands. This reduction is described by a Debye-Waller type factor (or Pekar-Huang-Reese factor in the theory of electron-phonon spectra) $\exp(-W)$. The parameter W is given by the integral of α_{sb} over ω ,

$$W = G_{\text{sb}} \bar{W}, \quad \bar{W} = 2a_{\parallel} \int dq q^{-4} F^2(q). \quad (33)$$

The dependence of the scaling factor \bar{W} on the field E_{\perp} and ω_{\parallel} is shown in Fig. 6. It is clear from this figure and Eq. (33) that W weakly depends on the in-plane electron frequency ω_{\parallel} as long as the corresponding ripplon frequency $\omega_r \ll k_B T/\hbar$. At the same time, W decreases with the increasing pressing field E_{\perp} , because the difference in the effective radii of the electron states $|1\rangle$ and $|2\rangle$ decreases, and so does the difference in the ripplon equilibrium positions in the states $|1\rangle$ and $|2\rangle$.

The calculated value of the Debye-Waller factor for electrostatically confined electrons $W \approx 0.1 - 0.05$ for $\omega_{\parallel}/2\pi = 20$ GHz) and E_{\perp} varying from 0 to ~ 300 V/cm) is close to the estimate $W \sim 0.05$ given earlier [15] for the case of in-plane confinement by a magnetic field. This factor emerges also in the analysis of the operation of a quantum computer based on trapped atomic ions [38], because optical transitions are connected to vibrational modes of the ions (the number of such modes is small, for a small number of ions).

In the context of quantum computing, sideband absorption and the Debye-Waller reduction of the zero-ripplon absorption strength differ qualitatively from electron decay and dephasing. The Debye-Waller mechanism does not affect an electron qubit between quantum operations. In contrast to dissipative effects, it does not accumulate between operations. However, it shows that a fraction of electron transitions may go wrong, as they are accompanied by excitation of ripples. The number of such transitions, and therefore the role of the

Debye-Waller factor, can be significantly reduced by using longer excitation pulses, as we will discuss in a separate publication.

VI. DECAY AND DEPHASING FROM COUPLING TO THE ELECTRODE

Coupling to the underlying electrode may also provide an important mechanism of relaxation of a confined electron (qubit). The corresponding relaxation parameters can be analyzed in a standard way. Fluctuations of the electrode potential modulate the inter-level distance and thus give rise to dephasing. In addition, an electron can make a transition between the states, with energy being transferred to an excitation in the electrode (for example, an electron-hole pair). The analysis is simplified by the fact that the size of the wave function of the qubit $\sim r_B$ is small compared to the distance to the electrode h . Then the interaction with the electrode can be described in dipolar approximation,

$$H_{\text{dip}} = -e \delta \hat{\mathcal{E}}_{\perp} z, \quad (34)$$

where $\delta \hat{\mathcal{E}}_{\perp}$ is the fluctuating part of the field on the electron normal to helium surface. This field comes from charge density fluctuations in the electrode. Here and below we do not consider effects of fluctuations of the electrode potential on in-plane motion, which are weak and not important for qubit dynamics.

Electron relaxation parameters can be expressed in terms of the correlation function of the fluctuating field

$$Q(\omega) = \int_0^{\infty} dt e^{i\omega t} \langle \delta \hat{\mathcal{E}}_{\perp}(t) \delta \hat{\mathcal{E}}_{\perp}(0) \rangle. \quad (35)$$

We will assume that the function $Q(\omega)$ is smooth in the frequency ranges of interest for dissipation effects, i.e. for either $\omega \lesssim k_B T / \hbar$ or $\omega \sim (E_2 - E_1) / \hbar$.

Field-induced time variation of the phase difference of the wave functions $|1\rangle$ and $|2\rangle$ comes from Stark shift and is equal to

$$\delta \phi_{12}(t) - \delta \phi_{12}(t') = \hbar^{-1} e (z_{22} - z_{11}) \int_{t'}^t d\tau \delta \hat{\mathcal{E}}_{\perp}(\tau).$$

Classical (thermal or quasi-thermal) field fluctuations give rise to phase diffusion on times that largely exceed the correlation time of $\delta \hat{\mathcal{E}}_{\perp}(t)$, which we assume to be short, $\lesssim \hbar / k_B T$. The coefficient of phase diffusion is equal to the dephasing rate $\Gamma_{\phi}^{(\text{el})}$. From Eq. (35)

$$\Gamma_{\phi}^{(\text{el})} = e^2 (z_{22} - z_{11})^2 \text{Re } Q(0) / \hbar^2. \quad (36)$$

If the noise spectrum $\text{Re } Q(\omega)$ has peaks at low frequencies $\omega \lesssim \Gamma_{\phi}^{(\text{el})}$, or the noise $\delta \hat{\mathcal{E}}_{\perp}(t)$ is non-Gaussian, decay of $\langle \exp[i\delta \phi_{12}(t)] \rangle$ becomes nonexponential. Although the analysis has to be modified in this case, it is still convenient to relate decoherence of electrons on helium to the fluctuating field $\delta \hat{\mathcal{E}}_{\perp}(t)$.

Decay rate of the qubit $\Gamma_{12}^{(\text{el})}$ is determined by the probability of a field-induced transition $|2\rangle \rightarrow |1\rangle$ between the electron states. This probability is determined, in turn, by quantum fluctuations of the field $\delta \hat{\mathcal{E}}_{\perp}(t)$ at frequency $\Omega_{12} = (E_2 - E_1) / \hbar$. From Eq. (35),

$$\Gamma_{12}^{(\text{el})} = e^2 |z_{12}|^2 \text{Re } Q(\Omega_{12}) / \hbar^2. \quad (37)$$

Here we assumed that decay is due to spontaneous emission only, i.e. that there are no induced processes with energy transfer $E_2 - E_1$.

To estimate relaxation parameters we will assume that the controlling electrode is a conducting sphere of a small radius r_{el} submerged at depth h beneath helium surface, as discussed in Sec. II. For low frequencies the surface of the sphere is equipotential. Then the fluctuating field of the electrode is simply related to its fluctuating potential $\delta \hat{V}_{\text{el}}$, $\delta \hat{\mathcal{E}}_{\perp} = \delta \hat{V}_{\text{el}} r_{\text{el}} / h^2$. Much of low-frequency noise is due to voltage fluctuations from an external lead attached to the electrode, which has resistance \mathcal{R}_{ext} and the temperature T_{ext} that largely exceeds the helium temperature T . The noise can be found from Nyquist's theorem and gives the dephasing rate

$$\Gamma_{\phi}^{(\text{el})} = 2k_B T_{\text{ext}} \mathcal{R}_{\text{ext}} e^2 (z_{22} - z_{11})^2 r_{\text{el}}^2 / \hbar^2 h^4. \quad (38)$$

For $\mathcal{R}_{\text{ext}} = 25 \text{ Ohm}$, $T_{\text{ext}} = 1 \text{ K}$, $r_{\text{el}} = 0.1 \mu\text{m}$, $h = 0.5 \mu\text{m}$, and $z_{22} - z_{11} = r_B$ we obtain $\Gamma_{\phi}^{(\text{el})} \approx 1 \times 10^4 \text{ s}^{-1}$. This shows that thermal electrode noise may be a major source of dephasing for a qubit. The requirement to keep this noise small may be important in determining the depth by which controlling electrodes can be submerged below helium surface.

In contrast to low-frequency noise, high-frequency voltage fluctuations from sources outside the thermostat can be filtered out. Much of high-frequency quantum fluctuations that affect a qubit come from the underlying microelectrode itself. They depend on the interrelation between the electron relaxation time τ_{el} in the electrode and Ω_{12}^{-1} . If $\tau_{\text{el}} \Omega_{12} \ll 1$, the electrode conductivity does not display dispersion up to frequencies $\gtrsim \Omega_{12}$; it greatly exceeds Ω_{12} for typical Ω_{12} .

An order-of-magnitude estimate of the decay rate $\Gamma_{12}^{(\text{el})}$ can be made by assuming that the controlling electrode is a lead attached to a sphere, and this sphere is equipotential (fluctuations of the total charge in the sphere make a major contribution to the field $\delta \hat{\mathcal{E}}_{\perp}$ for small r_{el}/h). Then from Nyquist's theorem

$$\Gamma_{12}^{(\text{el})} = 2(E_2 - E_1) \mathcal{R}_{\text{el}} e^2 |z_{12}|^2 r_{\text{el}}^2 / \hbar^2 h^4. \quad (39)$$

where \mathcal{R}_{el} is the resistance of the lead. If we estimate it as 0.1 Ohm , then using the same parameters as in the estimate of $\Gamma_{\phi}^{(\text{el})}$ and setting $E_2 - E_1$ equal to the ‘‘Rydberg’’ energy R (1), we obtain $\Gamma_{12}^{(\text{el})} \sim 5 \times 10^2 \text{ s}^{-1}$. Even though this estimate is very approximate, it is clear that the major effect of electrodes on qubit relaxation is dephasing rather than decay.

VII. CONCLUSIONS

In this paper we have provided a quantitative analysis of the parameters of qubits based on electrons on helium. We introduced a simple realistic model of electrodes, which are submerged into helium in order to localize and control the electrons. This model allowed us to estimate parameters of the electron energy spectrum and their dependence on the electrode potential. Control is performed by varying the field E_{\perp} normal to helium surface. This field changes the distance between the energy levels of a qubit, which are the ground and first excited levels of motion normal to the surface, and enables tuning qubits in resonance with each other and with externally applied microwave radiation.

The electrode potential determines not only E_{\perp} , but also the in-plane electron confinement. We found the frequency ω_{\parallel} of electron vibrations parallel to helium surface and related it to the field E_{\perp} . Typical frequencies $\omega_{\parallel}/2\pi$ are of order of a few tens of GHz, and typical fields are $\sim 100 - 300$ V/cm. We analyzed both the cases of one electrode and an electrode array, and investigated the effects of electrode geometry, including the inter-electrode distance and the depth by which electrodes are submerged into helium.

We identified relaxation mechanisms, estimated decay rates for a confined electron, and found their dependence on control parameters. In contrast to unconfined electrons studied before, decay is due primarily to electron transitions in which energy is transferred to two ripples propagating in opposite directions or to a bulk phonon propagating nearly normal to the surface. In both cases helium excitations with comparatively large wave numbers are involved. For different coupling mechanisms we have found the dependence of the decay rate on the parameters of a confined electron. The decay rate is essentially independent of temperature, for low temperatures.

The overall decay rate is of order 10^4 s^{-1} for typical ω_{\parallel} . This estimate is obtained assuming that the typical wave numbers of excitations into which an electron may scatter are $\lesssim 10^7 \text{ cm}^{-1}$. We expect that coupling to ripples and phonons with much shorter wave lengths is small. Then the decay rate can be significantly decreased if a magnetic field is applied perpendicular to helium surface, because such field leads to an increase in level spacing of in-plane electron excitations, and therefore more energetic helium excitations have to be involved in decay.

The major mechanism of dephasing due to coupling to excitations in helium is scattering of thermal ripples off an electron. We calculated the scattering rate and showed that it displays an unusual T^3 temperature dependence. The major contribution to the dephasing rate comes from processes which involve virtual transitions between electron states. The ripple-induced dephasing rate is $\sim 10^2 \text{ s}^{-1}$ for typical ω_{\parallel} and $T = 10 \text{ mK}$.

An important mechanism of dephasing is voltage fluctuations of controlling electrodes. The dephasing rate strongly depends on the source of these fluctuations and

also on the depth by which electrodes are submerged into helium. An estimate for Johnson noise from a typical lead connected to an electrode gives dephasing rate $\sim 10^4 \text{ s}^{-1}$.

We have also analyzed sidebands of electron absorption spectrum related to electron transitions accompanied by emission or absorption of a ripplon. We found the Debye-Waller factor which describes the intensity of the zero-ripplon absorption line and characterizes the overall probability of exciting a ripplon during an electron transition. This factor gives fidelity of qubit excitation by microwave radiation, which is a major single-gate operation of the quantum computer based on electrons on helium.

The results provide a quantitative basis for using electrons on helium as qubits of a quantum computer. The clock frequency of such computer Ω_{QC} , which is determined by the dipole-dipole inter-electron interaction, is in the range of $10^7 - 10^8 \text{ Hz}$ even for inter-electron distances $\approx 1 \mu\text{m}$, and therefore it largely exceeds both decay and dephasing rates of a confined electron. Our results suggest ways of further reduction of these rates. They show how to choose parameters of the system in an optimal way and also show that there is an extremely broad range where the parameters can be dynamically controlled, because the inter-level distance $E_2 - E_1 \gg \hbar\omega_{\parallel} \gg \hbar\Omega_{\text{QC}} \gg \hbar\Gamma$. They also suggest a sequence of steps that have to be done in order to implement a quantum computer with electrons on helium in experiment.

Acknowledgments

We are grateful to A. Dahm, B. Golding, and J. Goodkind for valuable discussions. This research was supported by the NSF through grant No. ITR-0085922.

APPENDIX: ONE-RIPPLON POLARONIC EFFECT

Besides relaxation, coupling to ripples leads also to a polaronic effect. Because ripplon frequencies are low, the major contribution comes from processes in which a ripplon is created or annihilated, but the state of the electron system is not changed. Polaronic shift of the electron transition frequency is then determined by the diagonal matrix elements of $H_i^{(1)}$ (9) on the wave functions $|1, 0, 0\rangle, |2, 0, 0\rangle$. Keeping only these terms in $H_i^{(1)}$ corresponds to the adiabatic approximation in which ripples have different equilibrium positions depending on the presence of an electron (one can think of a “dimple” made by an electron on helium surface [19]) and on the electron state. Of primary interest to us is the state dependence, as it characterizes the strength of coupling of the electron transition to ripples. The corresponding coupling is described by the Franck-Condon interaction

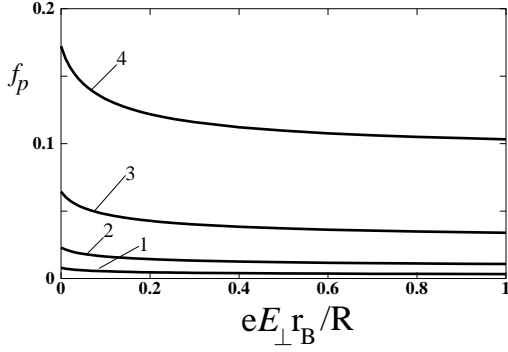


FIG. 7: The factor f_p in the Franck-Condon polaronic shift of the transition frequency of a qubit (A.1) as a function of the pressing field E_\perp for typical values of the in-plane localization length a_\parallel . The curves 1 to 4 correspond to $r_B/a_\parallel = 0.18, 0.25, 0.35, 0.5$; the respective values of $\omega_\parallel/2\pi$ are $\approx 10, 20, 39$, and 79 GHz.

Hamiltonian (31).

The Franck-Condon polaronic shift of the transition frequency $1 \rightarrow 2$ due to the coupling (31) is given by a simple perturbation theory,

$$P = P_{12}f_p(a_\parallel, E_\perp), \quad P_{12} = R^2/4\pi^2\hbar\sigma r_B^2, \quad (\text{A.1})$$

$$f_p = (4\pi\sigma/\rho)r_B^4 \int_0^\infty dq q^2 F^2(q) \omega_q^{-2},$$

where f_p is a dimensionless factor determined by the matrix elements of v_{pol} (10) on the wave functions of out-of-plane motion. It depends on the dimensionless parameters a_\parallel/r_B and $eE_\perp r_B/R$, and is numerically small for typical parameter values, see Fig. 7.

The numerical value of the factor P_{12} is $P_{12}/2\pi \approx 2.2 \times 10^7$ Hz. The energy $\hbar P_{12}$ is much less than the distance between the electron energy levels. The shift P is also smaller than the typical frequency ω_r of ripplons coupled to the electron (25). The inequality $|P| \ll \omega_r$ indicates that the $|1\rangle \rightarrow |2\rangle$ transition is weakly coupled to ripplons.

-
- [1] D. Loss and D.P. DiVincenzo, Phys. Rev. A **57**, 120 (1998).
 - [2] A. Imamoglu, D.D. Awschalom, G. Burkard, D.P. DiVincenzo, D. Loss, M. Sherwin, and A. Small, Phys. Rev. Lett. **83**, 4204 (1999).
 - [3] R. Vrijen, E. Yablonovitch, K. Wang, H-W. Jiang, A. Balandin, V. Roychowdhury, T. Mor and D. DiVincenzo, Phys. Rev. A **62**, 012306 (2000)
 - [4] B.E. Kane, Nature **393**, 133 (1998).
 - [5] T. D. Ladd, J. R. Goldman, F. Yamaguchi, Y. Yamamoto, E. Abe, K. M. Itoh, Phys. Rev. Lett. **89**, 017901 (2002)
 - [6] M.S. Sherwin, A. Imamoglu, and Th. Montroy, Phys. Rev. A **60**, 3508 (1999).
 - [7] G. Chen, N.H. Bonadeo, D.G. Steel, D. Gammon, D.S. Katzer, D. Park, and L.J. Sham, Science **289**, 1906 (2000).
 - [8] T.H. Stievater, X.Q. Li, D.G. Steel, D. Gammon, D.S. Katzer, D. Park, C. Piermarocchi, and L.J. Sham, Phys. Rev. Lett. **87**, 133603 (2001).
 - [9] V.D. Averin, Solid State Commun. **105**, 659 (1998).
 - [10] Y. Nakamura, Yu.A. Pashkin, and H.S. Tsai, Nature **398**, 786 (1999).
 - [11] J.R. Friedman, V. Patel, W. Chen, S.K. Tolpygo, and J.E. Lukens, Nature **406**, 43 (2000).
 - [12] C.H. van der Wal, A.C.J. ter Haar, F.K. Wilhelm, R.N. Schouten, C.J.P.M. Harmans, T.P. Orlando, S. Lloyd, and J.E. Mooij, Science **290**, 773 (2000).
 - [13] Y. Yu, S. Han, Xi Chu, S.-I. Chu, and Zh. Wang, Science **296**, 889 (2002).
 - [14] D. Vion, A. Aassime, A. Cottet, P. Joyez, H. Pothier, C. Urbina, D. Esteve, and M.H. Devoret, cond-mat/0205343.
 - [15] P.M. Platzman and M.I. Dykman, Science **284**, 1967 (1999).
 - [16] M.I. Dykman and P.M. Platzman, Quantum Information and Computation **1**, 102 (2001)
 - [17] K.R. Brown, D.A. Lidar, and K.B. Whaley, Phys. Rev. A **65**, 012307 (2002)
 - [18] D. DeMille, Phys. Rev. Lett. **88**, 067901 (2002).
 - [19] "Two dimensional electron systems on helium and other cryogenic substrates", ed. E.Y. Andrei (Kluwer, 1997).
 - [20] K. Shirahama, S. Ito, H. Suto, and K. Kono, J. Low Temp. Phys. **101**, 439 (1995).
 - [21] M.J. Lea, P.G. Frayne, and Yu. Mukharsky, Fortschr. Phys. **48** 1109 (2000)
 - [22] J.M. Goodkind and S. Pilla, Quantum Information and Computation **1**, 108 (2001).
 - [23] A. J. Dahm, J.M. Goodkind, I. Karakurt, and S. Pilla, J. Low Temp. Phys. **126**, 709, (2002).
 - [24] In the absence of in-plane confinement, electronic transitions between the states (1) and the Stark shift of the transition frequency were observed using microwave spectroscopy by C.C. Grimes, T.R. Brown, M.L. Burns, and C.L. Zipfel, Phys. Rev. B **13**, 140 (1976).
 - [25] J.M. Goodkind, private communication.
 - [26] E. Cheng, M.W. Cole, and M.H. Cohen, Phys. Rev. B **50**, 1136 (1994).
 - [27] M.M. Nieto, Phys. Rev. A **61**, 034901 (2000).
 - [28] M.A. Niesen and I.L. Chuang, *Quantum Computation and Quantum Information* (Cambridge University Press, Cambridge 2000).
 - [29] Recent experimental data on the ^4He liquid-vapor interface were obtained by K. Penanen, M. Fukuto, R.K. Heilmann, I.F. Silvera, and P.S. Pershan, Phys. Rev. B **62**, 9621 (2000). Quantum Monte Carlo simulations for symmetric helium films were done recently by E.W. Draeger and D.M. Ceperley, Phys. Rev. Lett. **89**, 015301 (2002).
 - [30] P.M. Platzman and G. Beni, Phys. Rev. Lett. **36**, 626 (1976).

- [31] M. Saitoh, J. Phys. Soc. Japan **42**, 201 (1977).
- [32] Yu.P. Monarkha and V.B. Shikin, Fiz. Nizk. Temp. **8**, 563 (1982)[Sov. J. Low Temp. Phys. **8**, 279 (1982)]
- [33] W. Hayes and A.M. Stoneham, *Defects and defect processes in nonmetallic solids* (Wiley, NY 1985).
- [34] M.I. Dykman, Phys. Stat. Sol. (b) **88**, 463 (1978).
- [35] Yu.P. Monarkha, Fiz. Nizk. Temp. **4**, 1093 (1978) [Sov. J. Low Temp. Phys. **4**, 515 (1978)].
- [36] D.O. Edwards, J.R. Eckardt, and F.M. Gasparini, Phys. Rev. A **9**, 2070 (1974).
- [37] A. Lastrì, F. Dalfovo, L. Pitaevskii, and S. Stringari, J. Low Temp. Phys. **98**, 227 (1995).
- [38] D.J. Wineland, C. Monroe, W.M. Itano, D. Leibfried, B.E. King, and D.M. Meekhof, J. Res. Natl. Inst. Stand. Technol. **103**, 259 (1998).